

# Kinematic Control of Redundant Robots with Online Handling of Variable Generalized Hard Constraints

Amirhossein Kazemipour\*, Maram Khatib\*, Khaled Al Khudir\*\*, Claudio Gaz\*\*\*, Alessandro De Luca\*

**Abstract**—We present a generalized version of the Saturation in the Null Space (SNS) algorithm for task control of redundant robots when hard inequality constraints are simultaneously present both in the joint and in the Cartesian space. These hard bounds should never be violated, are treated equally and in a unified way by the algorithm, and may also be varied, inserted or deleted online. When a joint/Cartesian bound saturates, the robot redundancy is exploited to continue fulfilling the primary task. If no feasible solution exists, an optimal scaling procedure is applied to enforce directional consistency with the original task. Simulation and experimental results on different robotic systems demonstrate the efficiency of the approach.

## I. INTRODUCTION

A robot manipulator is redundant with respect to a given task when the number of its joints is larger than that strictly needed to perform the task. The additional degrees of freedom allow for a greater flexibility in the execution of the primary task. Redundancy is usually exploited for achieving secondary goals, such as avoid collisions with workspace obstacles, maximize manipulability, stay away from kinematic singularities, or minimize energy consumption [1]. The presence of joint and Cartesian inequality constraints is a critical issue in redundancy resolution. Robots should comply with hard constraints on position, velocity and acceleration in their joint motion, typically due to limited joint ranges and actuator capabilities. Inequality constraints on the Cartesian motion may be present because of the nature of the task, sometimes suddenly appearing due to the unstructured environment in which the robot operates.

There are many ways to handle joint and Cartesian constraints in kinematic control of robots. Classical methods use artificial potentials [2], with a number of control points chosen along the kinematic chain being pushed away from the critical boundaries [3] and the associated control action taking place in the null space of the Jacobian of the primary task. This method is simple and effective, but highly parameter-dependent. Moreover, oscillatory behaviors may arise when activating/deactivating the evasive maneuvers in the proximity of the constraints [4]. In order to mitigate this undesired effect, the null-space projection term or the activation function may be designed in an incremental way [5], [6]. Nonetheless,

Manuscript received: February 24, 2022; Revised: May 28, 2022; Accepted: June 27, 2022.

This paper was recommended for publication by Editor Clement Gosselin upon evaluation of the Associate Editor and Reviewers' comments.

\*Dipartimento di Ingegneria Informatica, Automatica e Gestionale, Sapienza University of Rome, Roma, Italy. Emails: amrkzp@gmail.com, khatib@diag.uniroma1.it, deluca@diag.uniroma1.it

\*\*School of Mechanical, Aerospace and Automotive Engineering, Coventry University, Coventry, UK. Email: khaled.alkhudir@coventry.ac.uk

\*\*\*Faculty of Science, Engineering and Computing, Department of Mechanical Engineering, Kingston University, London, UK. Email: c.gaz@kingston.ac.uk

Digital Object Identifier (DOI): see top of this page.

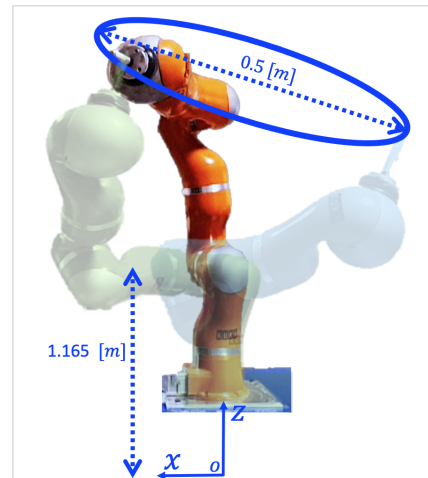


Figure 1: The KUKA LWR IV robot used for experimental evaluation. The world frame is placed on the lab floor. The desired end-effector task, the initial (solid orange), intermediate (shaded blue), and final (shaded orange) robot configurations of the first experiment are shown.

the selection of suitable gains is still required. Furthermore, when multiple tasks are present, incorporating the avoidance scheme into the original Stack of Tasks (SoT) will give to each inequality constraint a different priority [5]–[8].

In order to deal with joint positional constraints, a common approach is to transform hard joint bounds into soft constraints, by adopting a suitable cost function whose minimization will keep the joint motions close to the center of their admissible ranges [9]. Alternatively, a weighted pseudo-inverse technique can be used [10], which further penalizes joint motions when they approach their limits. These techniques, however, do not guarantee that the hard inequality constraints will be always satisfied, and so they may result in unfeasible solutions.

Over the last decade, constrained optimization methods have been applied to the inverse kinematics of redundant robots, transforming the given tasks into a Least Squares (LS) problem and looking for solutions in a feasible convex set. A general formulation within this paradigm, which extends the priority framework also to inequality tasks, has been presented in [11]. The LS formulation has the advantage of explicitly including hard bounds into a numerically solvable Quadratic Programming (QP) problem. It allows incorporating both joint and Cartesian motion limits as inequality constraints [12], [13]. However, these numerical approaches are computationally slower than analytical solutions [14]. Moreover, the feasibility of the task cannot be enforced, and the solution will be realizable only if the original (equality) task is compatible with the set of inequality constraints. Otherwise, the relaxation of these constraints in a least-square sense leads to a physical violation of the hard limits. As an alternative to the previously

mentioned QP approaches that minimize squared  $\ell_2$ -norms, using the  $\ell_1$ -norm minimization with suitable penalties offers a computationally efficient solution for hierarchical robot task control [15].

The Saturation in the Null Space (SNS) algorithm introduced in [16] is capable of resolving part of the issues raised earlier, by linking QP to the SoT approach. This framework provides a simple yet efficient solution to resolve robot redundancy at velocity, acceleration, or torque levels that can be combined into a single solver [17]. If strictly needed, the SNS method utilizes a suitable task-scaling mechanism to recover the feasibility of robot motion with respect to inequality constraints while preserving the geometric part of the primary equality task. This scaling strategy can be further extended in a predictive manner, by utilizing a model predictive control (MPC) approach to incorporate future evolution of the task [18]. In the original SNS algorithms, the inequality constraints on joint motion are regarded as hard bounds (i.e., they cannot be relaxed in a least-squares sense) and treated out of the SoT. So far, Cartesian bounds have not been treated explicitly, but rather approximated in the joint space as soft constraints. Accordingly, there is no guarantee that the robot will strictly comply also with the hard Cartesian constraints.

On the other hand, in [19] both joint and Cartesian inequality constraints have been taken explicitly into account in the SoT for torque-controlled manipulators. In this approach, hard joint limits should always be given the highest priority over all other constraints. However, when both Cartesian and joint constraints are violated, the algorithm becomes unreliable because other lower priority limits will be treated as soft constraints.

Building on our preliminary results in [20], we generalize the original SNS algorithm in [16] with the following contributions.

- A single augmented vector is defined that considers all joint and Cartesian inequality constraints explicitly. This vector can be adapted online, without any parameter tuning phase, to follow any desired modification (addition or removal) in the set of task constraints.
- In the proposed algorithm, presented here at the velocity command level, all joint/Cartesian inequality constraints are treated equally. Accordingly, the hard bounds are always respected strictly. This is independent of the primary task (or of the SoT and its related priority management, when considering multiple equality tasks).
- The primary task  $\dot{x}$  is relaxed optimally by keeping its geometric direction, if and only if no feasible solution exists. Differently from [16], if  $\dot{x}$  exceeds any Cartesian constraint, it is saturated to its associated limit.
- The algorithm applies the saturation technique in both the joint and the Cartesian space, unlike [16].

The resulting control algorithm can be viewed as a general tool that can be easily used in any robot application, such as human-robot collaboration tasks [21]. Its main feature is in fact an overall efficiency and the adaptability to time-varying hard constraints that may be generated or deleted online based on sensor information. The validation of the basic algorithm is carried out with different simulations and experiments (illustrated also in the accompanying video).

The rest of the paper is organized as follows. Section II introduces the framework for incorporating generalized con-

straints. In Sec. III, the new kinematic control algorithm is presented at the velocity command level. Simulation results on a planar 6R manipulator and experiments on the 7R KUKA LWR IV robot results are reported and discussed in Sec. IV. Conclusions are summarized in Sec. V.

## II. PROBLEM FORMULATION

Consider a robot manipulator with  $n$  joints and a single  $m$ -dimensional (primary) task  $x$ , with  $m < n$ , to be performed by its end effector (EE) and defined by

$$x = f(q), \quad J(q) = \frac{\partial f(q)}{\partial q}, \quad (1)$$

where  $q \in \mathbb{R}^n$  is the joint position vector and the  $m \times n$  task Jacobian matrix  $J$  has less rows than columns. Assuming that the robot is commanded by a kinematic control law at the velocity level, we solve the inverse kinematics as

$$\dot{q} = J^\#(q)\dot{x}, \quad (2)$$

where  $J^\#$  is the Moore–Penrose pseudoinverse of  $J$ . The command (2) is the minimum norm joint velocity corresponding to the desired task velocity  $\dot{x}$ . It is the preferred solution in the absence of the constraints, either in the joint or in the Cartesian space, that we shall consider next.

Define the position, velocity, and acceleration limits of each joint,  $j = 1, \dots, n$ , respectively as

$$\begin{aligned} Q_j^{min} &\leq q_j \leq Q_j^{max}, \\ V_j^{min} &\leq \dot{q}_j \leq V_j^{max}, \\ \Lambda_j^{min} &\leq \ddot{q}_j \leq \Lambda_j^{max}. \end{aligned} \quad (3)$$

Accordingly, inequality constraints can be defined at the velocity level for each joint  $j$  as

$$\begin{aligned} \dot{Q}_{min,j} &= \\ \max &\left\{ \frac{Q_j^{min} - q_j}{T}, V_j^{min}, -\sqrt{2\Lambda_j^{max}(q_j - Q_j^{min})} \right\}, \\ \dot{Q}_{max,j} &= \\ \min &\left\{ \frac{Q_j^{max} - q_j}{T}, V_j^{max}, \sqrt{2\Lambda_j^{max}(Q_j^{max} - q_j)} \right\}, \end{aligned} \quad (4)$$

where  $T$  is the sampling time. The velocity constraints in (4) is obtained by satisfying three requirements [16]: (1) the joint range limits should not be exceeded in the next sampled time instant; (2) the absolute joint velocity should be less than its specified limit; (3) the joint should be able to stop its motion before it reaches its closest joint range limit, assuming that the maximum feasible acceleration is applied.

Consider next  $r$  generic Cartesian control points distributed along the robot body, each of dimension  $d_{cp,i} \in \{1, 2, 3\}$ . Note that  $d_{cp,i}$  represents the number of Cartesian directions along which we constrain the motion. Accordingly, each control point (for  $i = 1, \dots, r$ ) can be limited in motion either in all directions ( $d_{cp,i} = 3$  in the 3D case,  $d_{cp,i} = 2$  in the 2D case) or in selected directions only (i.e.,  $d_{cp,i} < 3$  or  $d_{cp,i} < 2$ , respectively). The desired position, velocity, and acceleration limits for each control point  $i$  can be defined as

$$\begin{aligned} P_{cp,i}^{min} &\leq p_{cp,i} \leq P_{cp,i}^{max}, \\ V_{cp,i}^{min} &\leq \dot{p}_{cp,i} \leq V_{cp,i}^{max}, \\ \Lambda_{cp,i}^{min} &\leq \ddot{p}_{cp,i} \leq \Lambda_{cp,i}^{max}, \end{aligned} \quad (5)$$

where  $\mathbf{p}_{cp,i} \in \mathbb{R}^{d_{cp,i}}$  are the relevant position components of the  $i$ -th control point. As done in the joint space, inequality constraints can be defined for each control point velocity with

$$\begin{aligned} \dot{\mathbf{P}}_{cp,i}^{min} &= \\ \max &\left\{ \frac{\mathbf{P}_{cp,i}^{min} - \mathbf{p}_{cp,i}}{T}, \mathbf{V}_{cp,i}^{min}, -\sqrt{2\Lambda_{cp,i}^{max} (\mathbf{p}_{cp,i} - \mathbf{P}_{cp,i}^{min})} \right\}, \\ \dot{\mathbf{P}}_{cp,i}^{max} &= \\ \min &\left\{ \frac{\mathbf{P}_{cp,i}^{max} - \mathbf{p}_{cp,i}}{T}, \mathbf{V}_{cp,i}^{max}, \sqrt{2\Lambda_{cp,i}^{max} (\mathbf{P}_{cp,i}^{max} - \mathbf{p}_{cp,i})} \right\}, \end{aligned} \quad (6)$$

To take into account all the inequality constraints in (3) and (5) while executing the desired task  $\dot{\mathbf{x}}$ , we define the augmented vector (of dimension  $n + \sum_{i=1}^r d_{cp,i}$ )

$$\mathbf{a} = \left( \mathbf{q}^T \quad \mathbf{p}_{cp,1}^T \quad \mathbf{p}_{cp,2}^T \quad \dots \quad \mathbf{p}_{cp,r}^T \right)^T, \quad (7)$$

and the augmented  $(n + \sum_{i=1}^r d_{cp,i}) \times n$  matrix

$$\mathbf{A} = \left( \mathbf{I} \quad \mathbf{J}_{cp,1}^T \quad \mathbf{J}_{cp,2}^T \quad \dots \quad \mathbf{J}_{cp,r}^T \right)^T, \quad (8)$$

where  $\mathbf{I}$  is the  $n \times n$  identity matrix and  $\mathbf{J}_{cp,i}$  is the  $d_{cp,i} \times n$  Jacobian of the  $i$ -th control point position. Therefore, at a time instant  $t = t_l = lT$ , it is possible to define the generalized inequality constraints at the velocity level as

$$\mathbf{b}_{min}(t_l) \leq \dot{\mathbf{a}}(\mathbf{q}, \dot{\mathbf{q}}) \leq \mathbf{b}_{max}(t_l), \quad (9)$$

where  $\mathbf{b}_{min}$  and  $\mathbf{b}_{max}$  are the general limits augmented vectors and defined as

$$\begin{aligned} \mathbf{b}_{min} &= \left( \dot{Q}_{min,1} \dots \dot{Q}_{min,n} \quad \dot{\mathbf{P}}_{cp,1}^{min^T} \dots \dot{\mathbf{P}}_{cp,r}^{min^T} \right)^T, \\ \mathbf{b}_{max} &= \left( \dot{Q}_{max,1} \dots \dot{Q}_{max,n} \quad \dot{\mathbf{P}}_{cp,1}^{max^T} \dots \dot{\mathbf{P}}_{cp,r}^{max^T} \right)^T. \end{aligned} \quad (10)$$

Satisfying the generalized inequality constraints in (9) leads to impose the original position and velocity bounds in a strict sense, taking into account the acceleration limits. Note that, when the robot control law is defined at the velocity level, acceleration limits can be treated only as soft constraints.

Accordingly, the problem can be formulated as a QP subject to linear equality and inequality constraints as follows

$$\begin{aligned} \min_{\dot{\mathbf{q}} \in \mathbb{R}^n, s \in [0,1]} & \frac{1}{2} \dot{\mathbf{q}}^T \dot{\mathbf{q}} + \frac{1}{2} M(1-s)^2 \\ \text{s.t.} & \quad \mathbf{J} \dot{\mathbf{q}} = \dot{\mathbf{x}}, \quad \mathbf{b}_{min} \leq \mathbf{A} \dot{\mathbf{q}} \leq \mathbf{b}_{max} \end{aligned} \quad (11)$$

The parameter  $M \gg 1$  serves as a penalty factor and is used to favor the maximization of the task scaling factor  $s$  (ideally,  $s = 1$ ) over the minimization of the squared norm of the joint velocity  $\|\dot{\mathbf{q}}\|^2$ .

### III. THE GENERALIZED SNS ALGORITHM

We have revisited the original SNS algorithm in [16] so as to cover also the generalized constraints (9). We highlight here the main introduced differences.

The pseudo-code of the proposed scheme is presented as Algorithm 1. The method starts by initializing a projection matrix  $\mathbf{P} = \mathbf{I}$ , a null-space joint velocity vector  $\dot{\mathbf{q}}_N = \mathbf{0}$ , a scaling factor  $s^* = 0$ , a null-space augmented velocity vector  $\dot{\mathbf{a}}_N = \text{null}$ , and an augmented saturation matrix  $\mathbf{A}_{lim} = \text{null}$ .

On the basis of the minimum norm velocity solution, the current commanded joint velocity is given by

$$\dot{\mathbf{q}} = \dot{\mathbf{q}}_N + (\mathbf{J}\mathbf{P})^\# (\dot{\mathbf{x}} - \mathbf{J}\dot{\mathbf{q}}_N), \quad (12)$$

#### Algorithm 1 Generalized Saturation in the Null Space (GSNS)

```

1:  $\dot{\mathbf{q}}_N \leftarrow \mathbf{0}, s^* \leftarrow 0, \mathbf{P} \leftarrow \mathbf{I}, \mathbf{A}_{lim} \leftarrow \text{null}, \dot{\mathbf{a}}_N \leftarrow \text{null}$ 
2: repeat
   limits_violated  $\leftarrow$  FALSE
3:    $\dot{\mathbf{q}} \leftarrow \dot{\mathbf{q}}_N + (\mathbf{J}\mathbf{P})^\# (\dot{\mathbf{x}} - \mathbf{J}\dot{\mathbf{q}}_N)$ 
4:    $\dot{\mathbf{a}} \leftarrow \mathbf{A}\dot{\mathbf{q}}$ 
5:   if  $\exists h \in [1 : n + \sum_{i=1}^r d_{cp,i}] : (\dot{a}_h < b_{min,h}) \vee (\dot{a}_h > b_{max,h})$ 
     then
6:     limits_violated  $\leftarrow$  TRUE
7:      $\boldsymbol{\alpha} \leftarrow \mathbf{A}(\mathbf{J}\mathbf{P})^\# \dot{\mathbf{x}}$ 
8:      $\boldsymbol{\beta} \leftarrow \dot{\mathbf{a}} - \boldsymbol{\alpha}$ 
9:      $s_k \leftarrow \text{getTaskScalingFactor}(\boldsymbol{\alpha}, \boldsymbol{\beta})$ 
10:     $k \leftarrow \{\text{the most critical constraint}\}$ 
11:    if  $s_k > s^*$  then
12:       $s^* \leftarrow s_k$ 
13:       $\dot{\mathbf{q}}_N^* \leftarrow \dot{\mathbf{q}}_N, \mathbf{P}^* \leftarrow \mathbf{P}$ 
14:    end if
15:     $\mathbf{A}_{lim} \leftarrow \text{concatenate}(\mathbf{A}_{lim}, \mathbf{A}_k)$ 
16:     $\dot{\mathbf{a}}_N \leftarrow \begin{cases} \text{concatenate}(\dot{\mathbf{a}}_N, b_{max,k}) & \text{if } (\dot{a}_h > b_{max,k}) \\ \text{concatenate}(\dot{\mathbf{a}}_N, b_{min,k}) & \text{if } (\dot{a}_h < b_{min,k}) \end{cases}$ 
17:     $\mathbf{P} \leftarrow \mathbf{I} - (\mathbf{A}_{lim})^\# (\mathbf{A}_{lim})$ 
18:    if  $\text{rank}(\mathbf{J}\mathbf{P}) < m \wedge k \notin \{\text{primary task}\}$  then
19:       $\dot{\mathbf{q}} \leftarrow \dot{\mathbf{q}}_N^* + (\mathbf{J}\mathbf{P}^*)^\# (s^* \dot{\mathbf{x}} - \mathbf{J}\dot{\mathbf{q}}_N^*)$ 
20:      limits_violated  $\leftarrow$  FALSE
21:    end if
22:  end if
23:   $\dot{\mathbf{q}}_N \leftarrow (\mathbf{A}_{lim})^\# \dot{\mathbf{a}}_N$ 
24:  until limits_violated = TRUE
25:  $\dot{\mathbf{q}}_{SNS} \leftarrow \dot{\mathbf{q}}$ 

```

#### Algorithm 2 Optimal task scaling factor

```

function GETTASKSCALINGFACTOR( $\boldsymbol{\alpha}, \boldsymbol{\beta}$ )
1: for  $h \leftarrow 1 : n + \sum_{i=1}^r d_{cp,i}$  do
2:    $L_h \leftarrow b_{min,h} - \beta_h$ 
3:    $U_h \leftarrow b_{max,h} - \beta_h$ 
4:   if  $\alpha_h < 0 \wedge L_h < 0$  then
5:      $s_h \leftarrow L_h / \alpha_h$ 
6:   else
7:      $s_h \leftarrow 1$ 
8:   end if
9:   else if  $\alpha_h > 0 \wedge U_h > 0$  then
10:    if  $\alpha_h > U_h$  then
11:       $s_h \leftarrow U_h / \alpha_h$ 
12:    else
13:       $s_h \leftarrow 1$ 
14:    end if
15:  end if
16:  else
17:     $s_h \leftarrow 0$ 
18:  end if
19: end for
20:  $s \leftarrow \min s_h$ 
21: return  $s$ 
end function

```

which attempts to execute the desired task as efficiently as possible (with the lowest possible velocity norm) by enforcing the velocity of some overdriven joint/Cartesian constraints to saturation, thereby keeping the entire augmented velocity  $\dot{\mathbf{a}}$  in (9) within the desired constraints box. If the solution in (12) is acceptable under the constraints (9), the algorithm terminates and outputs this velocity for controlling the robot at the current time instant  $t_l$ . On the other hand, if it violates one or more of the hard generalized constraints, the algorithm repeats the loop until an admissible solution is found. This is accomplished by first calling Algorithm 2 to determine the most critical constraint  $k$ , which corresponds to a constraint that has the smallest scaling factor  $s_k$ , among all limits (see Fig. 2). Next, only the  $k$ -th joint/Cartesian constraint is saturated to its limit during each iteration, and  $\dot{\mathbf{a}}_N$  and  $\mathbf{A}_{lim}$  are updated accordingly. Then, the solution (12) is recomputed,

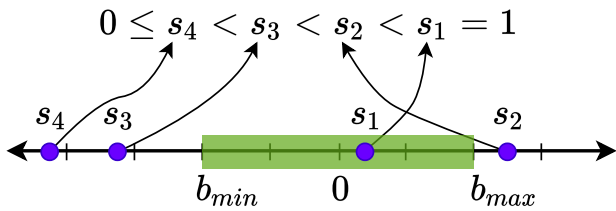


Figure 2: The task scaling factor associated with each constraint is computed in Algorithm 2. The factor is maximum (equal to 1 for the original task) when the corresponding velocity falls within the admissible interval, i.e.,  $b_{min,h} \leq \dot{a}_h \leq b_{max,h}$ . In all other cases, the scaling factor is less than 1, and the constraint becomes more critical as the associated velocity moves further away from the boundaries of the interval.

and the procedure is repeated.

At line 16,  $A_k$  corresponds to the  $k$ -row of the augmented matrix  $A$  defined in (8). At the current iteration, if the most critical constraint is associated with the  $k$ -th joint, then the  $k$ -th row of the identity matrix  $I_{n \times n}$  is extracted and augmented to  $A_{lim}$ . For the Cartesian constraints, a similar procedure is followed. For instance, if the most critical constraint is associated with the  $x$ -direction of the  $k$ -th control point, then the corresponding row of its Jacobian matrix  $J_{cp,k}^x$  is taken out and concatenated to  $A_{lim}$ .

At line 18, the projection matrix  $P$  is constructed according to the current saturated constraints as

$$P = I - (A_{lim})^\# (A_{lim}), \quad (13)$$

where  $A_{lim}$  incorporates the generalized active constraints.

At the end of each iteration, the algorithm checks if the robot is still redundant in executing the primary task under the currently active set of constraints ( $\text{rank}(JP) \geq m$ ). This check fails when the task redundancy of the robot is exhausted, and there is no way to perform  $\dot{x}$  under the given constraints. In this case, the solution with the largest task scaling factor obtained so far (the value  $s^* = s_k$  that is the closest to 1) is applied

$$\dot{q} = \dot{q}_N^* + (JP^*)^\# (s^* \dot{x} - J \dot{q}_N^*). \quad (14)$$

This choice preserves the geometry of the task, although it scales down the task speed by the (optimal) factor  $s^*$ .

Note that, if the current most critical constraint is associated with  $\dot{x}$ , i.e.,  $k \in \{\text{primary task}\}$ , e.g., when a control point coincides with the end-effector, then there is no need to scale down the task since its violated part is saturated to its limit, i.e., by modifying  $\dot{a}_N$  and  $A_{lim}$  accordingly. In this way, differently from [16], Algorithm 1 is able to saturate the constraints in both the joint and the Cartesian space. Finally, we remark that the proposed algorithm can be used to manage easily multiple Cartesian tasks with equal priority. This is essential for collision avoidance purposes when avoiding obstacles in the workspace is considered as a Cartesian task (see, e.g., [3]).

#### IV. NUMERICAL RESULTS

The efficiency of the new algorithm has been evaluated with simulations on planar manipulators, and with experiments on a 7R KUKA LWR IV robot. For the presented case studies, a stabilizing feedback action is integrated into the desired EE velocity  $\dot{x}$  of the primary task to compensate for any numerical errors as

$$\dot{x} = \dot{x}_d + K_p(x_d - f_{ee}(q)), \quad (15)$$

where  $x_d(\sigma)$  is the desired parametrized Cartesian path,  $\sigma(t)$  is the timing law of the path parameter,  $f_{ee}(q)$  is the robot direct kinematics, and  $K_p > 0$  is a (diagonal)  $m \times m$  control gain matrix. The actual motion of each considered robot is shown in the accompanying video.

#### A. Simulations

1) *6R planar manipulator*: A validation of Algorithm 1 has been done first through a MATLAB simulation. The EE of a 6R planar manipulator with unitary link lengths should track a 2D linear path ( $m = 2$ ) in  $T_{interval} = 10$  [s] with a rest-to-rest quintic polynomial as timing law, see Fig. 3. The control gain matrix is set to  $K_p = \text{diag}\{5, 5\}$  and the sampling time is  $T = 1$  [ms]. The initial robot configuration is chosen as

$$q_0 = (30 \quad -30 \quad -30 \quad 60 \quad -30 \quad -30)^T \text{ [deg]}. \quad (16)$$

In this example, the joint limits in (3) are equal and symmetric for all joints  $j = 1, \dots, 6$ , where

$$\begin{aligned} Q_j^{max} &= -Q_j^{min} = 90 \text{ [deg]}, \\ V_j^{max} &= -V_j^{min} = 15 \text{ [deg/s]}, \\ \Lambda_j^{max} &= -\Lambda_j^{min} = 30 \text{ [deg/s}^2]. \end{aligned} \quad (17)$$

As for Cartesian constraints, we considered  $r = 5$  control points (each with  $d_{cp,i} = 1$ ) along the robot body, located at the joints  $i = 2, \dots, 6$ . The Cartesian limits in (3) are the same for all control points, and are imposed only along the  $y$ -direction:

$$\begin{aligned} P_{cp,i}^{max,y} &= -P_{cp,i}^{min,y} = 1 \text{ [m]}, \\ V_{cp,i}^{max,y} &= -V_{cp,i}^{min,y} = 0.5 \text{ [m/s]}, \\ \Lambda_{cp,i}^{max,y} &= -\Lambda_{cp,i}^{min,y} = 1 \text{ [m/s}^2]. \end{aligned} \quad (18)$$

The EE begins its motion on the desired path, with no initial position error. As shown in Fig. 4, the trajectory error is kept to zero throughout task execution, except when the task scaling is active (i.e.,  $s^* < 1$ ) to comply with the saturated phases occurring in the joint and Cartesian motion—see Figs. 5 and 6. Note however that the desired geometric path for the end-effector in Fig. 3 is perfectly executed. The robot is capable of completing the primary task while satisfying all hard inequality constraints (many of which are saturated).

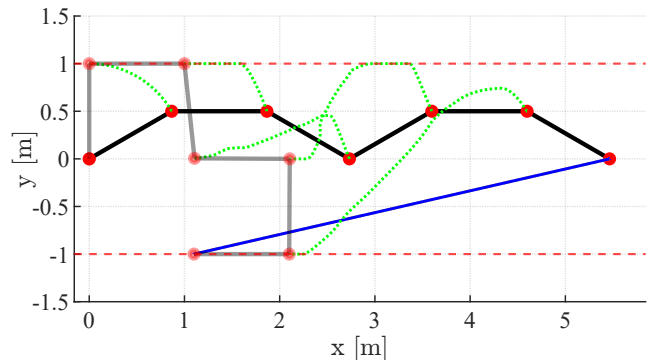


Figure 3: Simulation. The 6R planar arm is shown in its initial (black) and final (grey) configurations. The robot joints (and the end effector) are represented by red circles. The desired end-effector path is the blue line, to be traced from right to left. The Cartesian position limits are indicated by the two dashed red lines. The dotted green lines are the paths of the chosen control points during task execution.



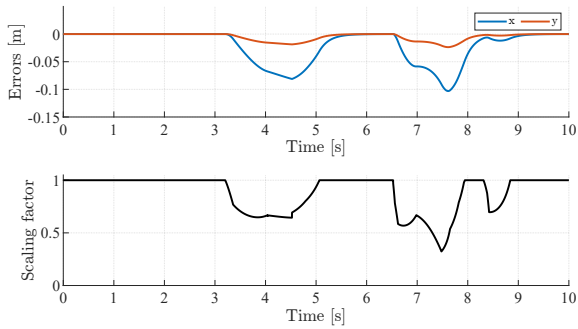


Figure 4: Simulation. End-effector trajectory tracking error components [top] and associated task scaling factor [bottom].

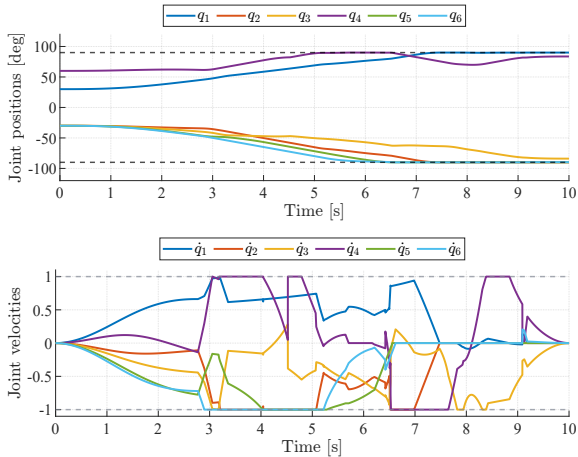


Figure 5: Simulation. Evolution of position [top] and velocity [bottom] of the joints during task execution. The limits on the joint motion are indicated by the dashed grey lines.

2) *Hyper-redundant planar manipulator*: In order to assess the computational efficiency of our algorithm, we considered a hyper-redundant planar robot having  $n$  revolute joints, with  $n$  varying from 20 to 200. The link lengths are chosen as  $l_j = 6/n$  [m], so that the total length of the robot is equal to that of the 6R planar manipulator of Fig. 3. The robot starts in the stretched configuration  $\mathbf{q} = \mathbf{0}$ , and its EE needs to track a 2D linear path in  $T_{interval} = 5$  [s] with a rest-to-rest quintic polynomial as timing law. In order to induce a large number of joint/Cartesian saturations during task execution, the joint

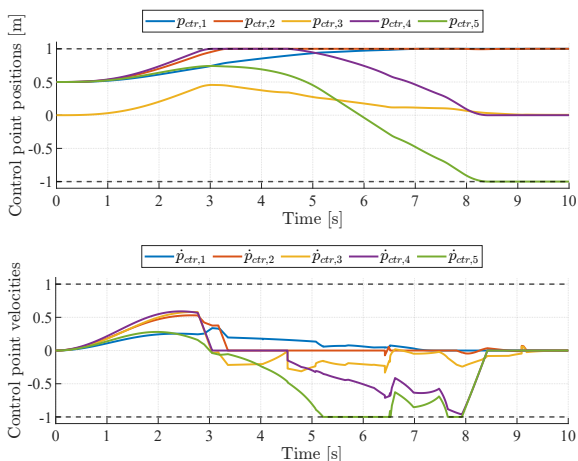


Figure 6: Simulation. Evolution of the position [top] and velocity [bottom] of the control points along the  $y$ -direction. The Cartesian limits on the motion of the control points are indicated by the dashed grey lines.

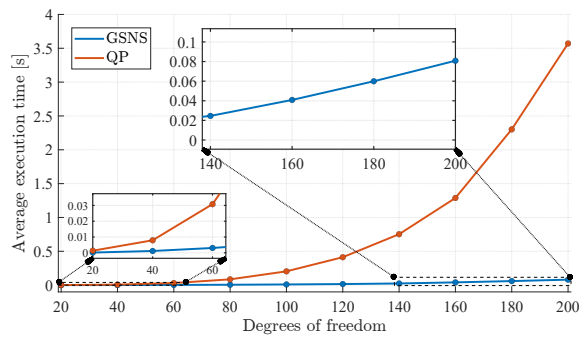


Figure 7: Simulation. Comparison of execution times with GSNS and with a local QP solver (qpOASES).

position limits are chosen as

$$Q_j^{max} = -Q_j^{min} = \frac{800}{n} \text{ [deg]}, \quad (19)$$

while the remaining joint and Cartesian constraints are the same as in (17) and (18).

For comparison, we benchmarked our algorithm (GSNS) against a state-of-the-art QP active-set solver *qpOASES* [22], which solves the optimization problem as formulated in (11). The simulations were conducted using MATLAB R2022a on an Intel Core i9-10900k CPU 3.7 GHz and 64 GB of RAM. The average execution times needed by the two algorithms are shown in Fig. 7. It can be clearly recognized that the GSNS consistently performs faster than *qpOASES*; the difference in execution times becomes larger as the number of degrees of freedom increases.

## B. Experiments with the KUKA LWR robot

The proposed Algorithm 1 has been implemented in C++ to perform experimental evaluations with a KUKA LWR IV robot with  $n = 7$  joints. The position control mode through the KUKA FRI library is used, with sampling time  $T = 5$  [ms]. The results of two experiments are presented.

1) *Cartesian constraints at the elbow*: In the first experiment, the desired EE task is to trace a slightly tilted 3D circle ( $m = 3$ ) for three rounds, starting on the path with the joint configuration

$$\mathbf{q}_0 = (13.50 \quad -7.76 \quad 55.16 \quad 79.70 \quad 0 \quad -6.19 \quad 0)^T \text{ [deg]}.$$

Defining the world frame on the laboratory floor (see Fig. 1), the desired circular path is centered at  $\mathbf{C} = (0 \quad 0.5 \quad 1.5)^T$  [m], with a radius of 0.25 [m]. The path timing law is a trapezoidal velocity profile, with cruise speed  $\dot{\sigma} = 0.15$  [m/s] and maximum acceleration  $\ddot{\sigma} = 0.15$  [m/s<sup>2</sup>]. The control gain is set to  $\mathbf{K}_p = \text{diag}(30, 30, 30)$  and the joint limits are

$$\begin{aligned} \mathbf{Q}^{max} &= -\mathbf{Q}^{min} = (170 \quad 105 \quad 170 \quad 120 \quad 170 \quad 85 \quad 170)^T \text{ [deg]}, \\ \mathbf{V}^{max} &= -\mathbf{V}^{min} = (20 \quad 22 \quad 20 \quad 26 \quad 26 \quad 36 \quad 36)^T \text{ [deg/s]}, \\ \mathbf{\Lambda}^{max} &= -\mathbf{\Lambda}^{min} = (30 \quad 30 \quad 30 \quad 30 \quad 30 \quad 30 \quad 30)^T \text{ [deg/s}^2\text{]}. \end{aligned}$$

A single control point of dimension  $d_1 = 2$  is considered at the robot elbow (joint 4), which has to satisfy the temporal constraints

$$\begin{aligned} p_{cpx} &\leq 0.15 \text{ [m]}, & 16 \leq t \leq 22 \text{ [s]}, \\ p_{cpy} &\leq 0.2 \text{ [m]}, & 5 \leq t \leq 10 \text{ [s]}, \end{aligned} \quad (20)$$

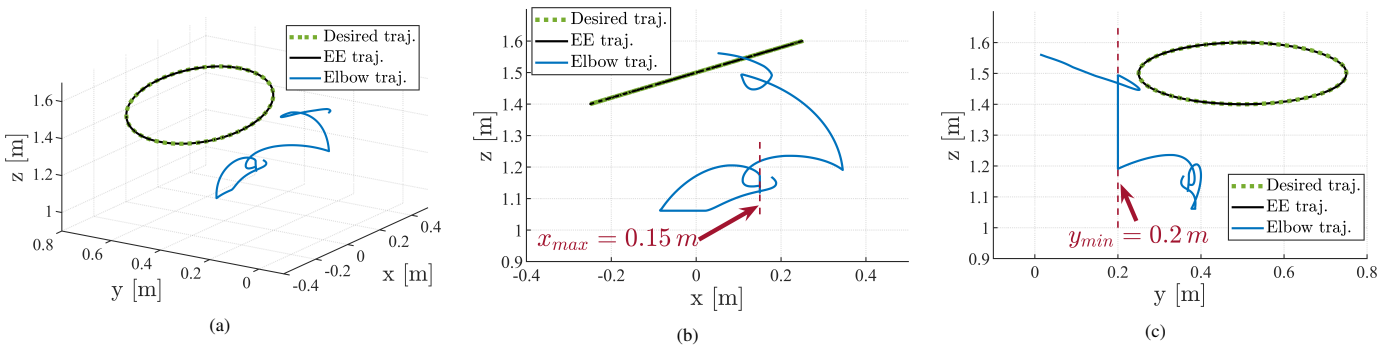


Figure 8: First experiment. (a) The path executed by the end effector (in black) coincides with the desired circle (dashed green). The position of the robot elbow (blue traces) satisfies the temporal constraints (20), both on the  $x$ -axis (b) and on the  $y$ -axis (c).

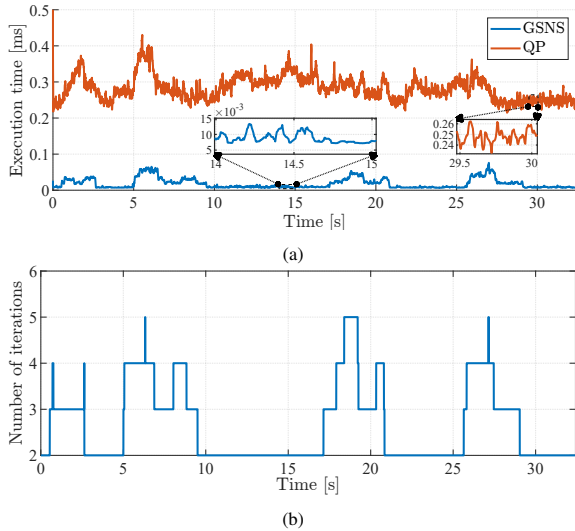


Figure 9: First experiment. (a) Comparison of execution times with GSNS and with a local QP solver (qpOASES). (b) Number of iterations for GSNS over time.

and the permanent constraints

$$\begin{aligned} -0.1 \leq \dot{p}_{cp_x} \leq 0.1, \quad -0.1 \leq \dot{p}_{cp_y} \leq 0.1 \text{ [m/s]}, \\ -0.5 \leq \ddot{p}_{cp_x} \leq 0.5, \quad -0.5 \leq \ddot{p}_{cp_y} \leq 0.5 \text{ [m/s}^2\text{]}. \end{aligned} \quad (21)$$

Figure 8 shows how the robot executes the desired task by complying with the Cartesian constraints. In Fig. 11(a), the trajectory error on the primary task is zero, except when no feasible solution exists under the considered hard constraints. In this case, the robot task is scaled down, i.e.,  $s^* < 1$ , while keeping the EE velocity direction tangent to the desired path. In fact, the EE motion in Fig. 8 keeps nicely the geometry of the original path.

The corresponding evolutions of the joints in Fig. 11(b) satisfy the hard joint limits at all times. The multiple saturation in position of joints 2, 3 and 6, as well as of all joint velocities (except for joint 7) clearly illustrates how Algorithm 1 exploits the available joint motion capabilities. The motion of the control point at the robot elbow is reported in Fig. 11(c). When the inequality constraints (20) are activated/deactivated (i.e., the shadowed areas), the elbow reacts properly and saturates, if necessary, to stay within the limits.

Figure 9(a) shows the execution time of our algorithm (GSNS) and of a local QP method (qpOASES), solving the optimization problem formulated in (11) with a penalty factor

of  $M = 10^3$ . Both algorithms are implemented as C++ codes. The results indicate that GSNS achieves a higher computational speed than qpOASES. Figure 9(b) shows the number of iterations performed by GSNS at each instant during task execution. As it can be seen, the execution time of the GSNS rises with the increase in the number of iterations. However, the GSNS average execution time is only  $18 \mu\text{s}$ , which is over an order of magnitude faster than that of qpOASES, running at  $283 \mu\text{s}$ .

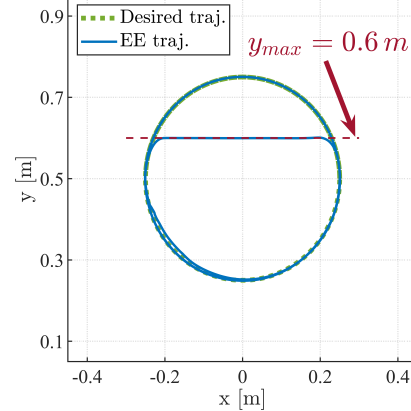


Figure 10: Second experiment. The end-effector path (in blue) coincides with the desired circle (dashed green) in the first and third rounds, while the EE position saturates the temporal constraint (22) during the second round.

2) *Cartesian constraints at the end-effector*: In the second experiment, a different control point of dimension  $d_1 = 2$  is chosen, which is coincident with the robot end effector. The primary task of dimension  $m = 3$  requires the EE to follow a circular path for three times as in the previous scenario, but the circle is now parallel to the  $xy$ -plane. The initial joint configuration is chosen as

$$\mathbf{q}_0 = (13.19 \ -8.59 \ 54.78 \ 89.04 \ -0.069 \ -10.09 \ 0)^T \text{ [deg]},$$

with the robot starting on the desired path. In this experiment, the maximum speed and acceleration of the EE trajectory have been raised to  $\dot{\sigma} = 0.65 \text{ [m/s]}$  and  $\ddot{\sigma} = 0.65 \text{ [m/s}^2\text{]}$ , respectively, in order to bring the robot closer to its physical limits. Accordingly, we use the (symmetric) joint limits provided by the manufacturer

$$\mathbf{Q}^{max} = (170 \ 120 \ 170 \ 120 \ 170 \ 120 \ 170)^T \text{ [deg]},$$

$$\mathbf{V}^{max} = (100 \ 110 \ 100 \ 130 \ 130 \ 180 \ 180)^T \text{ [deg/s]},$$

with  $\mathbf{Q}^{min} = -\mathbf{Q}^{max}$  and  $\mathbf{V}^{min} = -\mathbf{V}^{max}$ . Acceleration limits are  $\Lambda_j^{max} = -\Lambda_j^{min} = 300 \text{ [deg/s}^2\text{]}$ , for  $j = 1, \dots, 7$ .

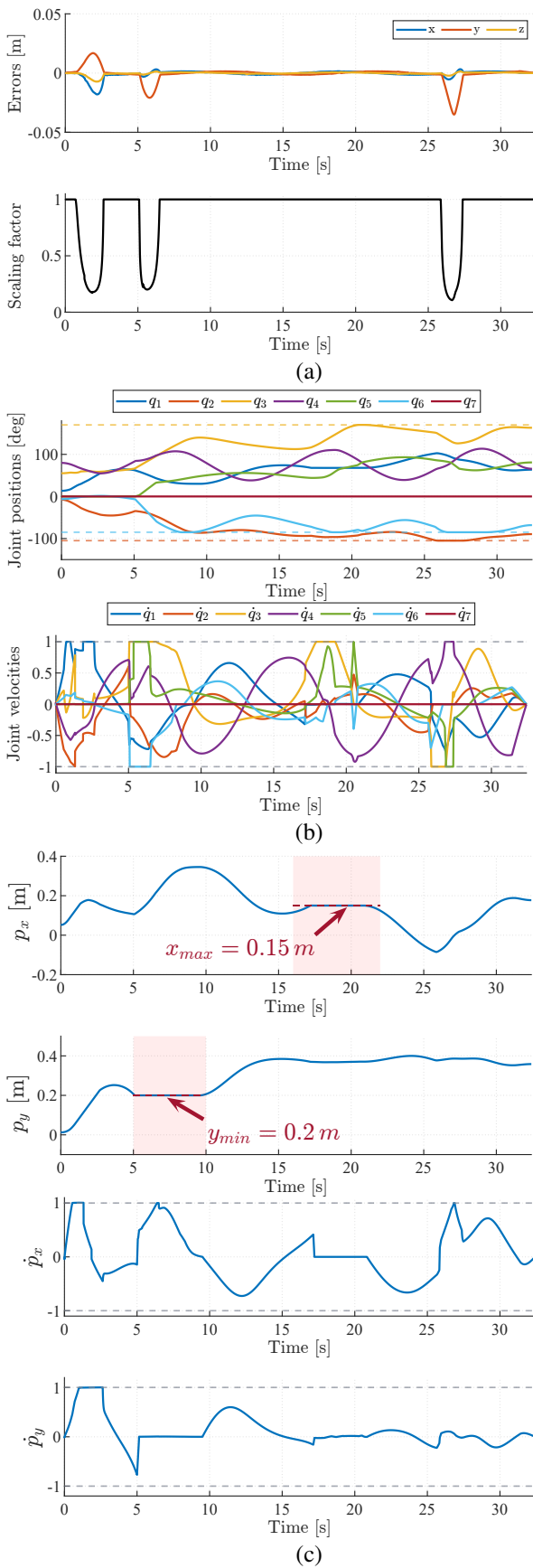


Figure 11: First experiment. (a) Trajectory error components on the primary task and related optimal scaling factor. (b) Joint positions and normalized velocities. (c) Elbow (control point) position and normalized velocity components. The shadowed areas in pink represent the activation period of the constraints (20). Dashed lines indicate the associated limits.

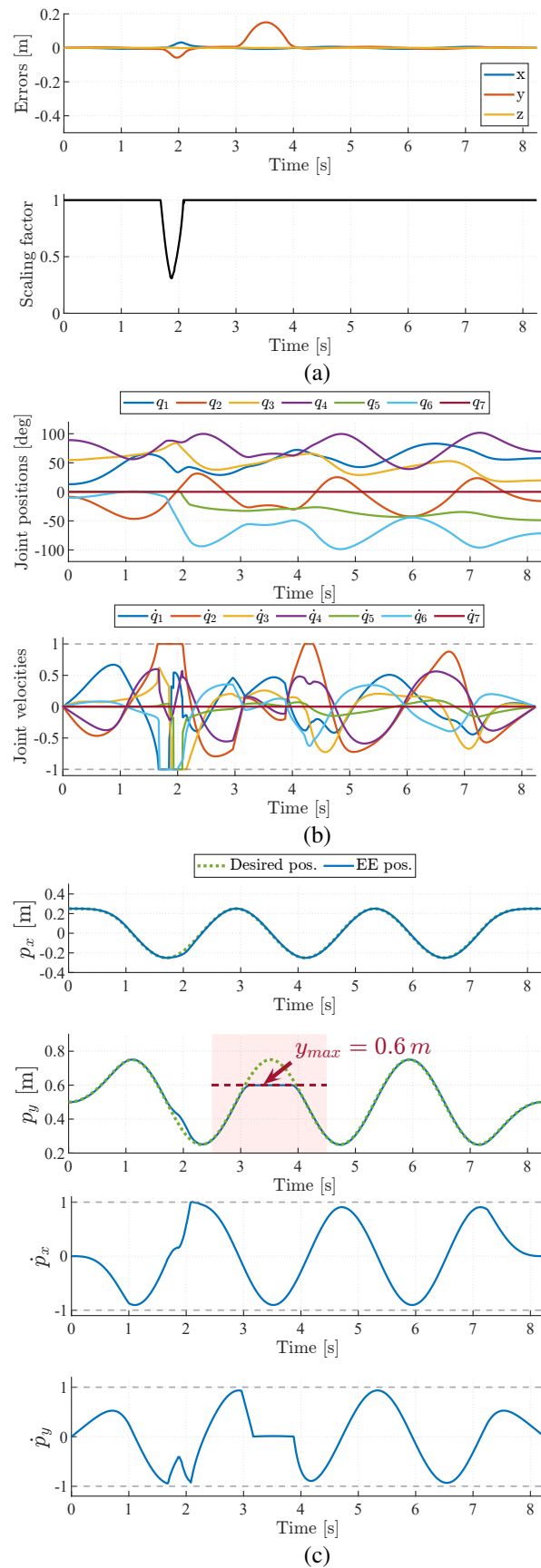


Figure 12: Second experiment. (a) Trajectory error components on the primary task and related optimal scaling factor. (b) Joint positions and normalized velocities. (c) End-effector (control point) position and normalized velocity components. The shadowed area in pink represents the activation period of the constraint (22). Dashed lines indicate the associated limits.

The temporal constraint

$$p_{cp_y} \leq 0.6 \text{ [m]}, \quad 2.5 \leq t \leq 4.5 \text{ [s]}, \quad (22)$$

is imposed to the control point together with the permanent constraints

$$\begin{aligned} -0.7 \leq \dot{p}_{cp_x} \leq 0.7, \quad -0.7 \leq \dot{p}_{cp_y} \leq 0.7 \text{ [m/s]}, \\ -1.5 \leq \ddot{p}_{cp_x} \leq 1.5, \quad -1.5 \leq \ddot{p}_{cp_y} \leq 1.5 \text{ [m/s}^2]. \end{aligned} \quad (23)$$

Figure 10 shows the execution of the task using Algorithm 1. In Fig. 12(a), the errors on the EE trajectory increase around  $t = 2$  [s], where the task scaling factor is applied in order to be able to satisfy the velocity limits of joints 1, 2 and 6 (see Fig. 12(b)). The EE error along the  $y$  direction between  $t = 3$  and  $t = 4$  [s] is large, because of the simultaneous activation of the (hard) temporal constraint (22), which is in fact inconsistent with the primary task. In this case, there is no use in scaling down the task as done instead in the former event. Moreover, while the EE position saturates at the imposed maximum limit in the  $y$ -direction, a complete fulfillment of the other task components along the  $x$  and  $z$  axes is still kept, see Fig. 12(c).

## V. CONCLUSIONS

We have presented a generalized null-space saturation algorithm for the kinematic control of redundant robots to realize a primary task under hard inequality constraints in the joint and Cartesian spaces. All hard constraints are equally enforced and the task is automatically scaled in an optimal fashion when no feasible solution exists. The presented case studies have proven the efficiency of the approach to handle any possible simultaneous (de-)activation of joint and/or Cartesian inequality constraints without any oscillatory behavior. The ability to handle time-dependent constraints makes the method easy to be integrated in any sensor-based strategy, e.g., for online/dynamic collision avoidance in human-robot collaborative applications [21]. As for the original SNS algorithm [16], one can consider moving the commands to the acceleration level, making them suitable for torque-controlled robotic systems. However, a proper extension of the velocity-based SNS technique to acceleration or torque levels requires further investigation since the task-scaling strategy at the acceleration level is not always sufficient to ensure the satisfaction of the geometrical path due to the additional kinematic terms that arise. Furthermore, the problem of hierarchical task control is not addressed in this work. Nevertheless, similar to the original SNS, the presented algorithm can be extended to include multiple operational tasks with priorities, keeping the entire set of hard inequality constraints out of the stack of equality tasks.

## REFERENCES

- [1] S. Chiaverini, G. Oriolo, and A. A. Maciejewski, "Redundant robots," in *Springer Handbook of Robotics*, B. Siciliano and O. Khatib, Eds. Springer, 2016, pp. 221–242.
- [2] O. Khatib, "Real-time obstacle avoidance for manipulators and mobile robots," in *Autonomous Robot Vehicles*, I. Cox and G. Wilfong, Eds. Springer, 1986, pp. 396–404.
- [3] M. Khatib, K. Al Khudir, and A. De Luca, "Task priority matrix at the acceleration level: Collision avoidance under relaxed constraints," *IEEE Robotics and Automation Lett.*, vol. 5, no. 3, pp. 4970–4977, 2020.
- [4] —, "Task priority matrix under hard joint constraints," in *Proc. 2nd Italian Conf. on Robotics and Intelligent Machines*, 2020, pp. 173–174.

- [5] N. Mansard, O. Khatib, and A. Kheddar, "A unified approach to integrate unilateral constraints in the stack of tasks," *IEEE Trans. on Robotics*, vol. 25, no. 3, pp. 670–685, 2009.
- [6] E. Simetti and G. Casalino, "A novel practical technique to integrate inequality control objectives and task transitions in priority based control," *J. of Intelligent and Robotic Systems*, vol. 84, no. 1, pp. 877–902, 2016.
- [7] L. Sentis and O. Khatib, "Synthesis of whole-body behaviors through hierarchical control of behavioral primitives," *Int. J. of Humanoid Robotics*, vol. 2, no. 4, pp. 505–518, 2005.
- [8] —, "A whole-body control framework for humanoids operating in human environments," in *Proc. IEEE Int. Conf. on Robotics and Automation*, 2006, pp. 2641–2648.
- [9] A. Liegeois, "Automatic supervisory control of the configuration and behavior of multibody mechanisms," *IEEE Trans. on Systems, Man, and Cybernetics*, vol. 7, no. 12, pp. 868–871, 1977.
- [10] T. F. Chan and R. V. Dubey, "A weighted least-norm solution based scheme for avoiding joint limits for redundant joint manipulators," *IEEE Trans. on Robotics and Automation*, vol. 11, no. 2, pp. 286–292, 1995.
- [11] O. Kanoun, F. Lamiroux, and P.-B. Wieber, "Kinematic control of redundant manipulators: Generalizing the task-priority framework to inequality task," *IEEE Trans. on Robotics*, vol. 27, no. 4, pp. 785–792, 2011.
- [12] A. Escande, N. Mansard, and P.-B. Wieber, "Hierarchical quadratic programming: Fast online humanoid-robot motion generation," *Int. J. of Robotics Research*, vol. 33, no. 7, pp. 1006–1028, 2014.
- [13] E. M. Hoffman, A. Laurenzi, L. Muratore, N. G. Tsagarakis, and D. G. Caldwell, "Multi-priority Cartesian impedance control based on quadratic programming optimization," in *Proc. IEEE Int. Conf. on Robotics and Automation*, 2018, pp. 309–315.
- [14] F. Flacco and A. De Luca, "Fast redundancy resolution for high-dimensional robots executing prioritized tasks under hard bounds in the joint space," in *Proc. IEEE/RSJ Int. Conf. on Intelligent Robots and Systems*, 2013, pp. 2500–2506.
- [15] A. S. Sathya, G. Pipeleers, W. Decré, and J. Swevers, "A weighted method for fast resolution of strictly hierarchical robot task specifications using exact penalty functions," *IEEE Robotics and Automation Letters*, vol. 6, no. 2, pp. 3057–3064, 2021.
- [16] F. Flacco, A. De Luca, and O. Khatib, "Control of redundant robots under hard joint constraints: Saturation in the null space," *IEEE Trans. on Robotics*, vol. 31, no. 3, pp. 637–654, 2015.
- [17] A. Ziese, M. D. Fiore, J. Peters, U. E. Zimmermann, and J. Adamy, "Redundancy resolution under hard joint constraints: A generalized approach to rank updates," in *Proc. IEEE/RSJ Int. Conf. on Intelligent Robots and Systems*, 2020, pp. 7447–7453.
- [18] M. Faroni, M. Beschi, N. Pedrocchi, and A. Visioli, "Predictive inverse kinematics for redundant manipulators with task scaling and kinematic constraints," *IEEE Transactions on Robotics*, vol. 35, no. 1, pp. 278–285, 2018.
- [19] J. D. M. Osorio, F. Allmendinger, M. D. Fiore, U. E. Zimmermann, and T. Ortmaier, "Physical human-robot interaction under joint and Cartesian constraints," in *Proc. 19th Int. Conf. on Advanced Robotics*, 2019, pp. 185–191.
- [20] A. Kazempour, M. Khatib, K. Al Khudir, and A. De Luca, "Motion control of redundant robots with generalised inequality constraints," in *Proc. 3rd Italian Conf. on Robotics and Intelligent Machines*, 2021, pp. 138–140.
- [21] M. Khatib, K. Al Khudir, and A. De Luca, "Human-robot contactless collaboration with mixed reality interface," *Robotics and Computer-Integrated Manufacturing*, vol. 67, p. 102030, 2021.
- [22] H. J. Ferreau, C. Kirches, A. Potschka, H. G. Bock, and M. Diehl, "qpOASES: A parametric active-set algorithm for quadratic programming," *Mathematical Programming Computation*, vol. 6, no. 4, pp. 327–363, 2014.